

# Effect of iron content and potassium substitution in $A_{0.8}Fe_{1.6}Se_2$ ( $A = K, Rb, Tl$ ) superconductors: a Raman-scattering investigation

A. M. Zhang, K. Liu, J. H. Xiao, J. B. He, D. M. Wang, G. F. Chen, B. Normand and Q. M. Zhang\*

*Department of Physics, Renmin University of China, Beijing 100872, P. R. China*

(Dated: December 19, 2018)

We have performed Raman-scattering measurements on high-quality single crystals of the superconductors  $K_{0.8}Fe_{1.6}Se_2$  ( $T_c = 32$  K),  $Tl_{0.5}K_{0.3}Fe_{1.6}Se_2$  ( $T_c = 29$  K), and  $Tl_{0.5}Rb_{0.3}Fe_{1.6}Se_2$  ( $T_c = 31$  K), as well as of the insulating compound  $KFe_{1.5}Se_2$ . To interpret our results, we have made first-principles calculations for the phonon modes in the ordered iron-vacancy structure of  $K_{0.8}Fe_{1.6}Se_2$ . The modes we observe can be assigned very well from our symmetry analysis and calculations, allowing us to compare Raman-active phonons in the AFeSe compounds. We find a clear frequency difference in most phonon modes between the superconducting and non-superconducting potassium crystals, indicating the fundamental influence of iron content. By contrast, substitution of K by Tl or Rb in  $A_{0.8}Fe_{1.6}Se_2$  causes no substantial frequency shift for any modes above  $60\text{ cm}^{-1}$ , demonstrating that the alkali-type metal has little effect on the microstructure of the FeSe layer. Several additional modes appear below  $60\text{ cm}^{-1}$  in Tl- and Rb-substituted samples, whose anomalous intensities suggest a freezing process in the A layer at low temperatures. Finally, our calculations reveal the presence of “chiral” phonon modes, whose origin lies in the chiral nature of the  $K_{0.8}Fe_{1.6}Se_2$  structure.

PACS numbers: 74.70.-b, 74.25.Kc, 63.20.kd, 78.30.-j

## I. INTRODUCTION

Iron pnictide superconductors display the highest superconducting transition temperatures yet known outside cuprate systems. Unsurprisingly, their discovery almost three years ago ignited an enduring drive both to search for new superconducting materials and to explore the fundamental physical properties of these systems, especially the pairing mechanism. Until recently, five such systems had been synthesized and studied, namely  $LnFeAsOF$  (known as “1111,” with  $Ln \equiv La, Ce, Pr, Nd, Sm, \dots$ ),<sup>1</sup>  $AFe_2As_2$  (“122,” with AE an alkaline earth),<sup>2</sup>  $AFeAs$  (“111,” with A an alkali metal),<sup>3</sup>  $Fe(Se,Te)$  (“11”),<sup>4</sup> and  $Sr_2VO_3FeAs$  (“21311”).<sup>5</sup>

FeSe is of particular interest among these systems for a number of reasons. The most important is that it does not contain the poisonous element As. In addition, however, its transition temperature,  $T_c$ , displays a very strong pressure dependence. At ambient pressure  $T_c \approx 8$  K,<sup>6</sup> much lower than in the 1111 and 122 systems, but a maximum  $T_c$  of 37 K can be reached under a pressure of approximately 6 GPa.<sup>7</sup> It has been shown<sup>6</sup> that the microscopic effect of the applied pressure is to alter the separation of the Se atoms from the Fe planes, and this very strong dependence opens the possibility of raising  $T_c$  by the introduction of internal chemical pressure. The first successful execution of this program was reported in Ref. 8, where a potassium-intercalated FeSe superconductor was synthesized and found to have  $T_c \approx 31$  K, a value comparable to that in the 122 materials. The compound was initially identified as being isostructural with  $BaFe_2As_2$ , and the apparent similarities between FeAs- and FeSe-based superconductors suggested that the new system might be a rather ordinary addition to the families of iron superconductors.

In parallel with intensive efforts to synthesize further examples of  $A_xFe_{2-y}Se_2$  systems, the electronic and magnetic properties of these compounds have been studied intensively. Infrared optical conductivity measurements indicated that the non-superconducting system is a small-gap semiconductor rather than a Mott insulator.<sup>9</sup> In superconducting samples, nuclear magnetic resonance (NMR) measurements found very narrow line widths, singlet superconductivity with no coherence peak, and only weak spin fluctuations.<sup>10</sup> Angle-resolved photoemission spectroscopy (ARPES) measurements<sup>11</sup> find one clear Fermi surface around the M point, and a full gap on this surface, but further details remain unclear. Both Raman<sup>12</sup> and infrared<sup>9</sup> spectroscopy find large numbers of phonon modes beyond those expected in a 122 structure, and transmission electron microscopy (TEM)<sup>13</sup> reveals a well-defined surface vacancy ordering.

The true nature of the  $A_xFe_{2-y}Se_2$  materials was revealed by neutron diffraction experiments.<sup>14</sup> First, these determine that the structure is dictated by a real Fe content of 1.6 in the superconducting crystals. This gives a regular, 1/5-depleted Fe vacancy ordering pattern with a  $\sqrt{5} \times \sqrt{5}$  unit cell. Second, the magnetic properties of the system are perhaps the most unusual of any known superconductor, featuring an ordered spin structure of antiferromagnetically coupled four-spin blocks, a very high Néel temperature of 520 K, and an extraordinarily large local moment of  $3.31\mu_B$  per Fe site.<sup>14</sup> The magnetic transition has now been confirmed by bulk measurements,<sup>15</sup> while Mössbauer spectroscopy has been used to verify the large local moment, giving results of 2.9 and  $2.2\mu_B$  in two separate studies.<sup>16</sup> These observations prove directly that the AFeSe superconductors are completely different from FeAs-based and cuprate superconductors in at least two respects. One is the apparent coexistence of

long-range antiferromagnetic order with superconductivity. The other is that a bulk ordering of the Fe vacancies plays a key role in determining the electronic and magnetic properties of the system.

Returning to the question of sample synthesis, rapid progress followed the first report of  $K_xFe_{2-y}Se_2$ , with several groups achieving superconductivity by substitution of alkali-type metals including Rb, Cs, and Tl.<sup>17</sup> The purpose of substitution by ions of equal valence but different radii is to alter the chemical pressure to control the electronic properties. An example is the maximum  $T_c$  of approximately 56 K achieved by the substitution of rare-earth ions in the 1111 system.<sup>18</sup> It is thus somewhat surprising that substitution of K by Rb, Cs, or Tl in the new superconductors leaves  $T_c$  essentially unaltered at around 30 K.<sup>17</sup> This result poses another fundamental question concerning why superconductivity should be so robust in the AFeSe system, and its answer requires a careful investigation into the effect of Tl, Rb, and Cs substitution on the microstructure of the FeSe layers in these new materials.

In this paper, we address these questions through a Raman-scattering study. We have measured the spectra in three high-quality superconducting crystals of Tl- and Rb-substituted  $K_{0.8}Fe_{1.6}Se_2$ , and in one non-superconducting crystal with an altered Fe content. For each crystal, we observe double-digit numbers of phonon modes, dramatically different from a normal 122 structure but consistent with an ordered vacancy structure. We perform first-principles calculations for the zone-center phonon modes in  $K_{0.8}Fe_{1.6}Se_2$  ( $T_c = 32$  K) in order to assign the observed modes by the symmetries and frequencies we measure, resulting in a very satisfactory assignment. From this understanding, we find the effect of a varying Fe content to be detectable as frequency shifts of the Raman modes above  $60\text{ cm}^{-1}$ , as these are vibrations involving Fe and Se atoms. By contrast, the effects of Tl and Rb substitution are not discernible above  $60\text{ cm}^{-1}$ , indicating that K-layer substitution causes no substantial distortion of the FeSe layer. However, additional modes below  $60\text{ cm}^{-1}$  can be observed in the substituted samples and we find anomalous behavior at low temperatures, which suggests an explanation in terms of a freezing of atomic positions within the A layers. In our calculations we also find some unconventional ‘‘chiral’’ phonon modes, which arise due to the chiral nature of the  $\sqrt{5} \times \sqrt{5}$  Fe-vacancy structure, and we consider their implications for coupling to possible chiral electronic and magnetic modes.

## II. MATERIALS AND METHODS

The FeSe-based crystals used in our measurements were grown by the Bridgeman method. The detailed growth procedure may be found elsewhere.<sup>19</sup> The accurate determination of crystal stoichiometry has been found to be a delicate issue, which is crucial in estab-

lishing the proper starting point for understanding the new superconductors. We have obtained highly accurate results for our crystal compositions by using inductively coupled plasma atomic emission spectroscopy (ICP-AES), and have obtained results completely consistent with the neutron diffraction refinement.<sup>14</sup> The crystals we used in this study were  $K_{0.8}Fe_{1.6}Se_2$  ( $T_c \approx 32$  K),  $Tl_{0.5}K_{0.3}Fe_{1.6}Se_2$  ( $T_c \approx 29$  K), and  $Tl_{0.5}Rb_{0.3}Fe_{1.6}Se_2$  ( $T_c \approx 31$  K), all of which were superconducting with similar transition temperatures, and also the non-superconducting compound  $KFe_{1.5}Se_2$ . The precise chemical formula for this series of compounds has been found to be  $A_xFe_{2-x/2}Se_2$  ( $A = K, Rb, Cs, Tl$ ),<sup>20</sup> and our results agree with this deduction. X-ray diffraction patterns obtained for some of the crystals show no discernible secondary phases. The resistivities of the samples were measured with a Quantum Design physical properties measurement system (PPMS), and the magnetization by using the PPMS vibrating sample magnetometer (VSM). Sharp superconducting and diamagnetic transitions are found for all three superconducting crystals. These results indicate that all of the crystals used in our Raman measurements are of very high quality.

All measurements were made by cleaving the crystals in a glove box, to obtain flat, shiny (*ab*)-plane surfaces. The freshly-cleaved crystals were sealed under an argon atmosphere and transferred into the cryostat within 30 seconds for immediate evacuation to a work vacuum of approximately  $10^{-8}$  mbar. Raman-scattering measurements were performed with a triple-grating monochromator (Jobin Yvon T64000) in a pseudo-backscattering configuration. The beam of the 532 nm solid-state laser (Torus 532, Laser Quantum) was focused into a spot on the sample surface with a diameter of approximately  $20\ \mu\text{m}$ . The beam power was reduced to avoid heating, and was kept below 0.6 mW during our measurements at the lowest temperatures; the real temperature in the spot was deduced from the intensity relation between the Stokes and anti-Stokes spectra.

## III. FIRST-PRINCIPLES DYNAMICAL ANALYSIS

A full understanding of our Raman-scattering results, and in particular of the effects caused by iron content and potassium substitution, requires a complete phonon mode assignment. The ordered pattern of Fe vacancies<sup>14</sup> explains quite naturally the large number of optical phonons observed in light-scattering experiments. However, the large unit cell means that a detailed vibration analysis is somewhat involved. We begin with the results from neutron diffraction,<sup>14</sup> which gives the structural space group of  $K_{0.8}Fe_{1.6}Se_2$  as  $I4/m$  and the Wyckoff positions of the atoms as 8h for potassium, 16i for iron, 4d for the iron vacancies, and 16i for selenium. The corresponding symmetry analysis allows a total of  $17 A_g$  or  $B_g$  modes.<sup>12</sup>

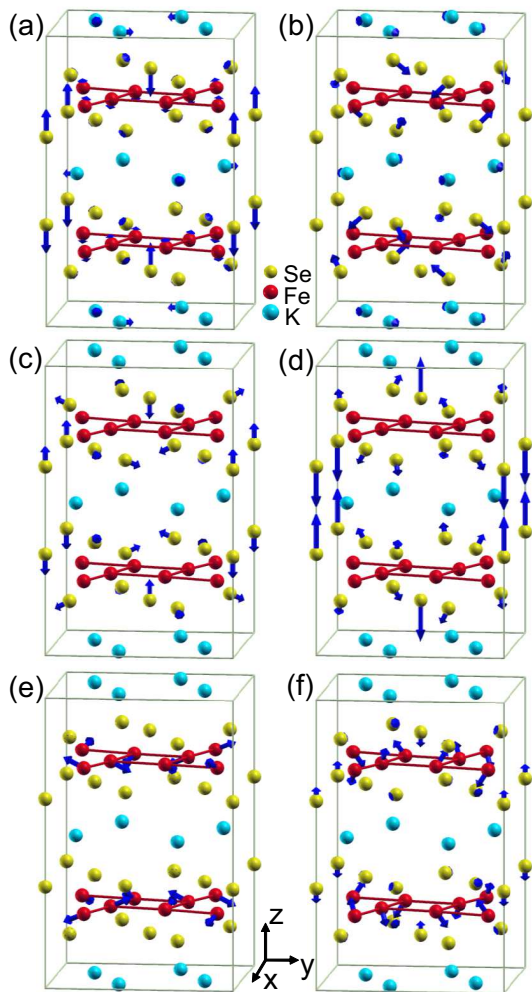


FIG. 1: (Color online) Atomic displacement patterns for selected Raman-active  $A_g$  modes of  $K_{0.8}Fe_{1.6}Se_2$ , with frequencies of (a) 75.1, (b) 130.5, (c) 159.2, (d) 212.6, (e) 268.5, and (f) 286.1  $cm^{-1}$ . Fe atoms connected by red lines have right-handed chirality in this representation.

We have calculated the nonmagnetic electronic structure and the zone-center phonons of  $K_{0.8}Fe_{1.6}Se_2$  from first principles by performing density-functional calculations. We use the Vienna *ab-initio* simulation package,<sup>21,22</sup> which makes use of the projector augmented wave (PAW) method<sup>22</sup> combined with a general gradient approximation (GGA), implemented with the Perdew-Burke-Ernzerhof formula,<sup>23</sup> for the exchange-correlation potentials. The nonmagnetic  $K_{0.8}Fe_{1.6}Se_2$  system was modeled by adopting a parallelepiped supercell containing 8 Fe atoms plus 2 Fe vacancies, 10 Se atoms, and 4 K atoms plus 1 K vacancy. The Brillouin zone of the supercell was sampled with an  $8 \times 8 \times 8$   $\mathbf{k}$ -space mesh and the broadening was taken to be Gaussian. The energy cutoff for the plane waves was 400 eV. Both the shape and volume of the cell and the internal coordinates of all ions were fully optimized until the forces on all relaxed atoms were below 0.01 eV/Å.

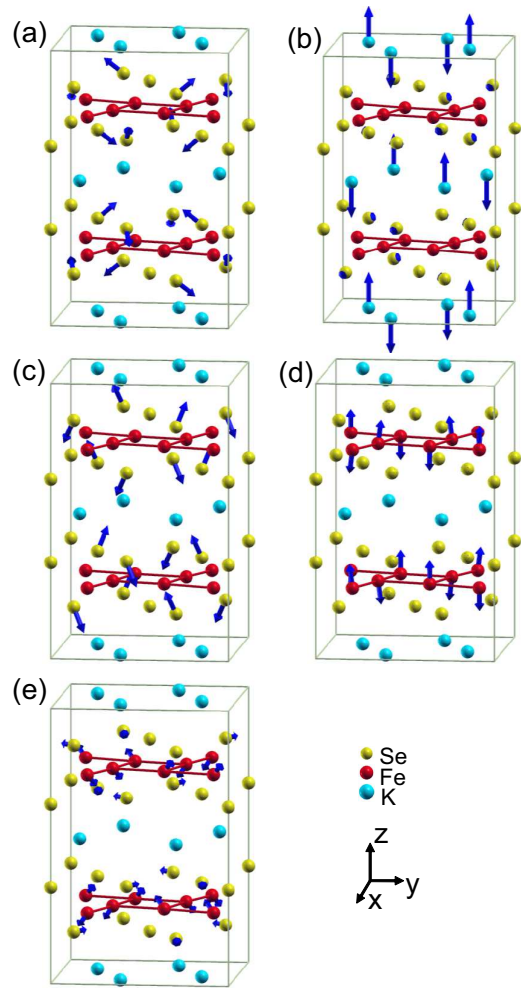


FIG. 2: (Color online) Atomic displacement patterns for selected Raman-active  $B_g$  modes of  $K_{0.8}Fe_{1.6}Se_2$  with frequencies of (a) 66.7, (b) 106.2, (c) 149.0, (d) 238.3, and (e) 279.0  $cm^{-1}$ . Fe atoms connected by red lines have right-handed chirality.

The frequencies and displacement patterns of the phonon modes were calculated using the dynamical matrix method,<sup>24</sup> in which the derivatives were taken from the finite differences in atomic forces at given atomic displacements of 0.01 Å. All 22 atoms in the supercell were allowed to move from their equilibrium positions in all directions ( $x, y, z$ ), leading to a  $66 \times 66$  matrix. The phonon frequencies and displacement patterns are given by diagonalizing this matrix. Convergence tests carried out by comparing the different  $\mathbf{k}$ -points assured that the final results were well converged both in their overall energetics and in the phonon spectrum (yielding accuracies of order  $\sim 2$   $cm^{-1}$ ). The 22-atom supercell has 63 optical modes. For the purposes of illustration, the displacement patterns of the phonon modes, deduced from real-space translational invariance, are shown in the 44-atom  $I4/m$  cell.

The calculated phonon frequencies are listed in Ta-

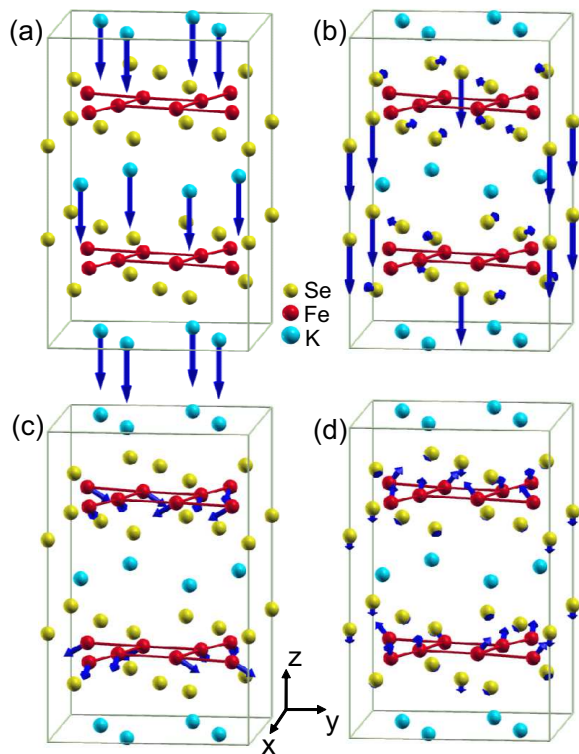


FIG. 3: (Color online) Atomic displacement patterns for selected infrared-active phonon modes of  $\text{K}_{0.8}\text{Fe}_{1.6}\text{Se}_2$  with frequencies of (a) 119.1, (b) 212.3, (c) 253.4, and (d) 308.5  $\text{cm}^{-1}$ . Fe atoms connected by red lines have right-handed chirality.

ble I. The experimental frequencies in the left-hand column are discussed in Sec. IV. As expected, the majority of the modes are vibrations related to the Fe and Se atoms in the primary structural unit, with vibrations of K atoms appearing only at low energies. The atomic displacement patterns of the assigned  $A_g$  and  $B_g$  modes are shown respectively in Figs. 1 and 2. In addition to the Raman-active modes, the optical phonons we have calculated also contain a number of infrared-active modes, also listed in Table I, and the displacement patterns for four selected examples are illustrated in Fig. 3. As for the Raman-active modes, most of the infrared modes are also vibrations of the Fe and Se atoms.  $\text{K}_{0.8}\text{Fe}_{1.6}\text{Se}_2$  can be considered as an ordered, 1/5-depleted version of the tetragonal “122” iron arsenide superconductors, in which there exist just two ideal, one-dimensional Raman-active phonon modes, whose symmetries are  $A_{1g}$  and  $B_{1g}$ .<sup>25</sup> It is clear that the symmetry reduction and expansion of the unit cell compared to the 122 system allows many more Raman- and infrared-active optical modes to exist in the new FeSe superconductors.

It is worth noting that in our calculations we also find some novel “chiral” phonon modes, whose atomic displacement patterns are shown in Fig. 4. These are modes in which all the Fe or Se atoms in a single plane of the structural unit have a net rotation about the center of the cell, an apparent moment canceled by the atomic dis-

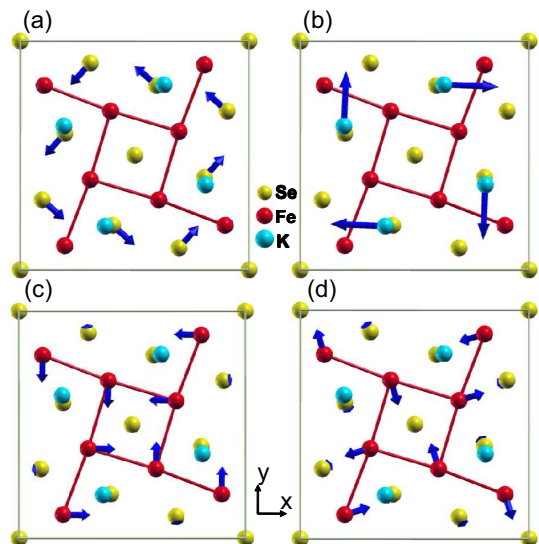


FIG. 4: (Color online) Atomic displacement patterns for chiral phonon modes [(a) 67.0, (b) 86.2, and (c) 301.3  $\text{cm}^{-1}$ ] and for the breathing mode [(d) 269.6  $\text{cm}^{-1}$ ] of  $\text{K}_{0.8}\text{Fe}_{1.6}\text{Se}_2$ . Fe atoms connected by red lines have right-handed chirality.

placements in the other FeSe layer of the unit cell. The presence of these chiral modes is a direct consequence of chiral symmetry breaking in the AFeSe system when the 1/5-depleted vacancy structure is adopted; the  $\sqrt{5} \times \sqrt{5}$  unit cell<sup>14</sup> itself has an explicit left- or right-handed structural chirality. The chiral phonon modes are not active in the Raman channel, and therefore are not observed in the Raman measurements performed here. We suggest, however, that these chiral modes may be observed by different spectroscopic techniques in circular polarization configurations.

TABLE I: Assignment of observed Raman-active modes ( $A_g$  and  $B_g$ ) and selected infrared modes ( $A_u$ ) in  $\text{K}_{0.8}\text{Fe}_{1.6}\text{Se}_2$

Expt. Freq. ( $\text{cm}^{-1}$ )	Cal. Freq. ( $\text{cm}^{-1}$ )	Symmetry	Atoms	Index
61.4	66.7	$B_g$	Se	$^1B_g$
66.3	75.1	$A_g$	K, Fe, Se	$^1A_g$
100.6	106.2	$B_g$	K	$^2B_g$
123.8	130.5	$A_g$	K, Se	$^2A_g$
134.6	159.2	$A_g$	Se	$^3A_g$
141.7	149.0	$B_g$	Se	$^3B_g$
202.9	212.6	$A_g$	Se	$^4A_g$
214.3	238.3	$B_g$	Fe	$^4B_g$
239.4	268.5	$A_g$	Fe	$^5A_g$
264.6	286.1	$A_g$	Fe, Se	$^6A_g$
274.9	279.0	$B_g$	Fe, Se	$^5B_g$
	119.1	$A_u$	K	
	212.3	$A_u$	Se	
	253.4	$A_u$	Fe	
	308.5	$A_u$	Fe, Se	

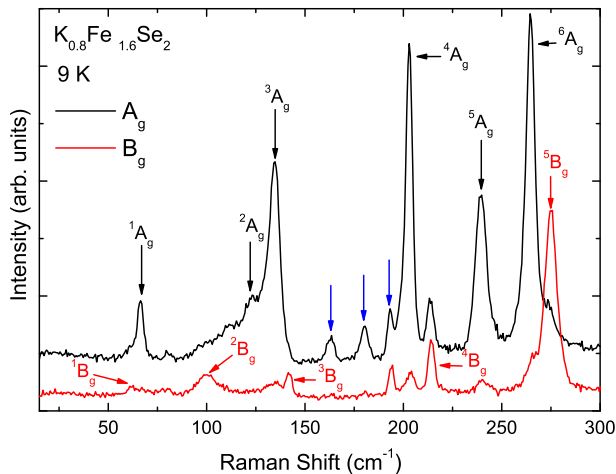


FIG. 5: (Color online) Raman spectra for  $\text{K}_{0.8}\text{Fe}_{1.6}\text{Se}_2$ , measured in the  $A_g$  and  $B_g$  channels at 9 K. The mode assignment is made on the basis of the symmetry analysis and the first-principles calculations of Sec. III. The corresponding atomic displacement patterns can be found in Figs. 1 and 2. Blue arrows indicate unassigned modes.

The presence of chiral modes is of particular interest as a possible probe of chiral electronic or magnetic excitations, which break time-reversal symmetry. Such excitations have been discussed in the parent compounds of cuprate superconductors, where an  $A_2$  component attributed to chiral spin excitations was detected by Raman scattering.<sup>26</sup> At the theoretical level, a chiral  $d$ -density-wave state has also been proposed in the underdoped state of cuprate superconductors.<sup>27</sup> Such modes, involving chiral electronic motion, may couple preferentially to the chiral phonon vibration in the  $1/5$ -depleted AFeSe system, in the same way as phonons of  $B_{1g}$  symmetry couple to the  $d$ -wave order parameter in cuprates, and thus Raman phonon spectroscopy may be used to detect their presence. Without such a coupling to phonon modes, any chiral electronic or magnetic excitations in the AFeSe system may also be subject to direct detection by the polarized spectroscopies, such as ARPES and neutron scattering, also applied in the study of cuprates.

#### IV. RAMAN-SCATTERING MEASUREMENTS

The low-temperature Raman spectra of  $\text{K}_{0.8}\text{Fe}_{1.6}\text{Se}_2$  are shown in Fig. 5. The measurements were performed at 9 K in polarization configurations which separate the  $A_g$  and  $B_g$  channels. At least fourteen Raman-active modes are observed both in this and in the other K-substituted samples (Fig. 8). All modes are located below  $300 \text{ cm}^{-1}$  and differ little in location between samples. Infrared measurements reporting more than ten modes<sup>9</sup> are also consistent with the analysis of Sec. III. This abundance of optical modes arises due to the symmetry reduction caused by Fe vacancy ordering, which

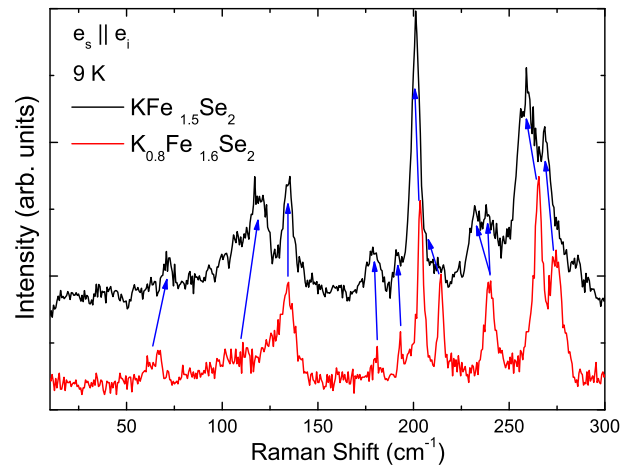


FIG. 6: (Color online) Comparison between Raman spectra of  $\text{K}_{0.8}\text{Fe}_{1.6}\text{Se}_2$  and  $\text{KFe}_{1.5}\text{Se}_2$ . Labels  $e_i$  and  $e_s$  denote respectively the polarizations of the incident and scattered light.

we have identified as being from  $D_{4h}$  to  $C_{4h}$ .<sup>12</sup> The space group of the undepleted, 122-type structure,  $I4/mmm$ , is reduced to  $I4/m$ , a process in which all in-plane, two-fold rotation axes and all mirror planes perpendicular to the  $(ab)$ -plane are lost. The phonon modes observed in the polarized Raman spectra of Fig. 5 are in excellent agreement with the calculations of Sec. III for the spectrum of optical modes (Table I).

#### A. Fe content

In Fig. 6 we compare the Raman modes in superconducting  $\text{K}_{0.8}\text{Fe}_{1.6}\text{Se}_2$  with those in non-superconducting  $\text{KFe}_{1.5}\text{Se}_2$ . The modes in the two samples show a general similarity in intensity and location, which implies a similarity in the microstructures and symmetries of their FeSe layers. However, it is also evident that changing the Fe content causes an obvious shift in frequency for most of the modes. Because these modes are vibrations involving the Fe and Se ions (Table I), this reflects some significant differences between the FeSe layers in the two samples. As noted above, neutron diffraction confirms that the system with an Fe stoichiometry of 1.6 (20% Fe vacancies) forms the ideal, four-fold-symmetric,  $1/5$ -depleted,  $\sqrt{5} \times \sqrt{5}$  vacancy-ordering pattern. The same pattern is also suggested<sup>14</sup> for the sample with an Fe content of 1.5 (25% Fe vacancies), but with the 16i iron positions partially occupied. This occupation means a random distortion of the Fe-Se bonds, which is responsible for the shifts in mode frequencies. Our results are thus in agreement with those from neutron diffraction, confirming that the electronic and magnetic properties of the AFeSe system are rather sensitive to the microstructure of the FeSe layers, which can be controlled through the Fe content. In fact, changing the Fe content from 1.6 to 1.5 causes this sample to become an insulator with

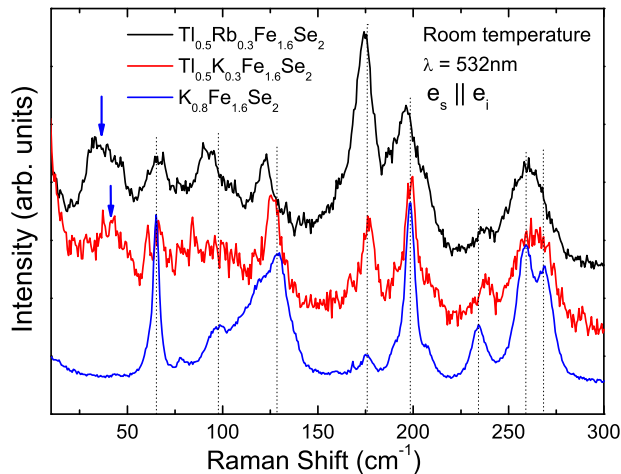


FIG. 7: (Color online) Raman spectra of the three superconducting crystals at room temperature. Additional modes, indicated by blue arrows, appear below  $60 \text{ cm}^{-1}$  in the Tl- and Rb-substituted samples. Dotted lines are guides indicating the peak positions.

a small gap, which is estimated by infrared experiments to be  $30 \text{ meV}$ ,<sup>9</sup> and by transport measurements to be approximately  $80 \text{ meV}$ .<sup>14</sup>

### B. K substitution

Raman spectra for the three superconducting crystals  $\text{K}_{0.8}\text{Fe}_{1.6}\text{Se}_2$ ,  $\text{Tl}_{0.5}\text{K}_{0.3}\text{Fe}_{1.6}\text{Se}_2$ , and  $\text{Tl}_{0.5}\text{Rb}_{0.3}\text{Fe}_{1.6}\text{Se}_2$  are shown in Fig. 7. In contrast to the case of changing Fe content discussed above, the modes above  $60 \text{ cm}^{-1}$  exhibit no substantial shift in frequency (although there are clear differences in relative intensities). This suggests that substitution within the potassium layers (at fixed Fe content) has little effect on the FeSe layer, and essentially none on the ordering pattern of the Fe vacancies. This substitution does, however, cause certain other changes to occur. The most notable is the presence of some additional phonon modes, which appear below  $60 \text{ cm}^{-1}$ . These modes can be attributed unambiguously to vibrations of the heavier Tl and Rb ions, which are absent in the spectra of  $\text{K}_{0.8}\text{Fe}_{1.6}\text{Se}_2$  (Figs. 5 and 6) and  $\text{KFe}_{1.5}\text{Se}_2$  (Figs. 6 and 8). The other important alteration is the dramatic intensity enhancement of the mode at  $180 \text{ cm}^{-1}$ , which has  $A_g$  character but cannot (Fig. 5) be assigned well from the calculations of Sec. III; we discuss this feature in detail below.

The additional, low-frequency modes induced by K-substitution show an anomalous temperature-dependence (Fig. 8). These become weaker but not narrower with decreasing temperature, eventually disappearing at  $9 \text{ K}$ . This behavior is similar to that of the  $66 \text{ cm}^{-1}$  Se  $A_g$  mode, which is also quite anomalous.<sup>12</sup> No structural transition is found below the Néel temperature ( $520 \text{ K}$ ) in neutron-diffraction studies of  $\text{K}_{0.8}\text{Fe}_{1.6}\text{Se}_2$ ,<sup>14</sup>

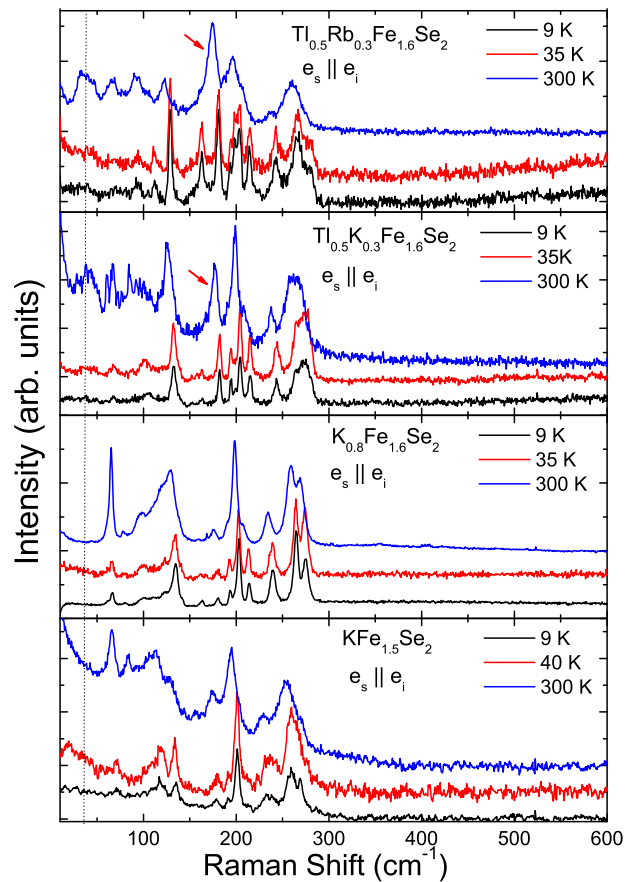


FIG. 8: (Color online) Raman spectra of superconducting and non-superconducting AFeSe systems at selected temperatures. The dotted line indicates the location of additional modes induced by K substitution and the red arrows indicate modes showing large changes of intensity between different crystals.

and the temperature-dependent Raman spectra in Fig. 8 show that it is reasonable to assume the same behavior in the Tl- and Rb-substituted crystals. We therefore deduce that the additional modes are prohibited at low temperatures due to changes of the local symmetry in the (Tl,K/Rb)-layer, for which a freezing of the A ions with decreasing temperature is the most likely possibility. In the absence of ionic or covalent bonds, the link between the ions in the intercalated A layer and the FeSe layers is weak. Our results are consistent with the ions being more mobile at higher temperatures, but becoming static, presumably in a random pattern, at lower temperatures. It should also be noted here that there exist two possible Wyckoff positions for the A ions, namely 2a and 8h, and that no Raman-active modes are allowed for atoms in the 2a positions.

The  $T$ -dependence of the  $66 \text{ cm}^{-1}$  phonon mode may also be interpreted within the framework of an A-ion freezing. This mode is a  $c$ -axis displacement of the Se ions, which brings these particularly close to the potential of both the Fe and the A ions. When the latter are

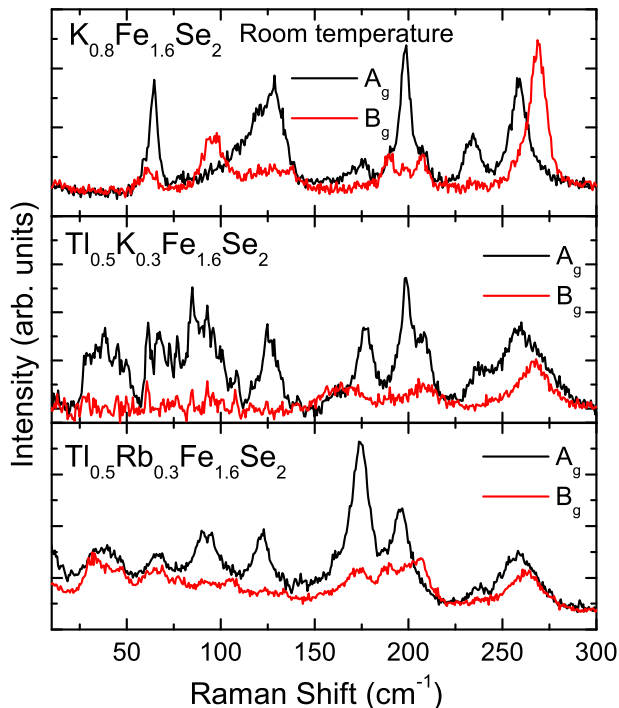


FIG. 9: (Color online) Polarized Raman spectra of the three superconducting crystals, showing that phonon widths are generally lower in  $\text{K}_{0.8}\text{Fe}_{1.6}\text{Se}_2$ .

uniformly distributed, the mode may behave in a conventional manner, whereas a freezing of the A ions may act to destroy the local force-field responsible for the mode. Thus it is the mode intensity which falls away, rather than the mode frequency showing an anomalous temperature-dependence. Further, the Se ion plays a key role in electronic hopping processes between next-nearest-neighbor Fe ions by p-d orbital overlap in the FeSe layer. This exchange integral is modulated by  $c$ -axis displacement of the Se ions, and the jump observed in the  $66\text{ cm}^{-1}$  mode intensity at the superconducting transition ( $T_c$ ) reflects this connection between the lattice and the electronic state.

Returning to the anomalous  $180\text{ cm}^{-1}$  mode, this shows not only a curious temperature-dependence of its intensity between samples, but also of its frequency at  $T_c$ . The fact that this mode cannot be assigned properly by our symmetry analysis and first-principles calculations suggests that it may be a local mode. One of the most likely candidates for this would be a nanoscopic region where the Fe vacancy is filled, creating a locally regular square lattice. Indeed the  $A_{1g}$  mode in the 122 compounds does occur close to  $180\text{ cm}^{-1}$ , which would imply that the local mode is also a  $c$ -axis displacement of Se. In this scenario, the jump in mode frequency at  $T_c$  suggests a strong coupling between the local modes and the symmetry of the order parameter. The results of Fig. 7 suggest further that A-induced changes in the local microstructure can act to alter the mode intensity

in the same way as for the  $66\text{ cm}^{-1}$  mode.

We comment also on the distinctive low-energy background observed for the four crystals we have measured (Fig. 8). The spectrum of semiconducting  $\text{KFe}_{1.5}\text{Se}_2$  at room temperature rises strongly at low frequencies, whereas the low-energy part for  $\text{K}_{0.8}\text{Fe}_{1.6}\text{Se}_2$  is rather flat. All of the background contributions fall with decreasing temperature. We suggest that the low-frequency enhancement may be due to electronic Raman scattering. Because  $\text{KFe}_{1.5}\text{Se}_2$  is a small-gap semiconductor, the smaller Coulomb screening effect relative to a normal metal would allow stronger charge density fluctuations and hence a larger electronic Raman scattering contribution.

One of the most surprising features of the  $\text{K}_{0.8}\text{Fe}_{1.6}\text{Se}_2$  system is its apparently high degree of structural order, despite being of a depleted nature obviously prone to atomic disorder. Evidence for disorder can be found in the polarized Raman spectra at room temperature (Fig. 9). The Tl- and Rb-substituted samples show larger phonon widths compared to  $\text{K}_{0.8}\text{Fe}_{1.6}\text{Se}_2$ , which implies that more disorder is induced by the substitution. Given that no substantial shifts occur in the mode frequencies for the three samples, this disorder can be attributed to the random occupation and motion of the K, Tl, and Rb ions. The breaking of local symmetry and periodicity in the A layer acts to shorten the phonon lifetimes also in the FeSe layer.

Before concluding this discussion, we note also that, in seeking an explanation for the minor anomalies present in our results (the unassigned modes, some temperature-dependences), we cannot exclude the possibility of microscale phase separation occurring at sufficiently low temperatures. There remains to date no evidence for the presence of secondary phases in X-ray and neutron-scattering studies,<sup>14,28</sup> and the diamagnetic transition at the onset of superconductivity is remarkably sharp in the  $\text{K}_{0.8}\text{Fe}_{1.6}\text{Se}_2$  sample.<sup>12</sup> Such a phase separation, if present, would not explain these anomalies, presenting instead a different scenario in which to understand not only the phonon spectrum but also the entire nature of superconductivity and magnetism in the intriguing new FeSe superconductors.

## V. SUMMARY

To conclude, we have measured Raman spectra in single-crystalline samples of the new superconductors  $\text{K}_{0.8}\text{Fe}_{1.6}\text{Se}_2$ ,  $\text{Tl}_{0.5}\text{K}_{0.3}\text{Fe}_{1.6}\text{Se}_2$ , and  $\text{Tl}_{0.5}\text{Rb}_{0.3}\text{Fe}_{1.6}\text{Se}_2$ , as well as in their insulating derivative compound  $\text{KFe}_{1.5}\text{Se}_2$ . A symmetry analysis and first-principles calculations of the zone-center phonons, both based on the  $\sqrt{5} \times \sqrt{5}$  vacancy-ordering pattern of the  $\text{K}_{0.8}\text{Fe}_{1.6}\text{Se}_2$  unit cell, allow an excellent assignment of the observed phonon modes. We illustrate the corresponding atomic displacement patterns and demonstrate the presence of chiral phonon modes.

We observe a clear frequency shift in all phonons between superconducting  $\text{K}_{0.8}\text{Fe}_{1.6}\text{Se}_2$  and non-superconducting  $\text{KFe}_{1.5}\text{Se}_2$ , showing the effect of further Fe vacancies within the  $\sqrt{5} \times \sqrt{5}$  structure on the microscopic properties of the FeSe layers. By contrast, the frequencies of modes involving Fe and Se ions are little affected on substituting K by Tl or Rb. However, this substitution does induce additional Tl and Rb modes below  $60 \text{ cm}^{-1}$ . The additional modes become much weaker at low temperatures, which suggests a freezing of atomic positions within the (Tl,K/Rb) layer. Our measurements reveal the complex effects of Fe vacancies in the new superconductors, which result in a series of distinct structural, electronic, and magnetic properties. These lay the foundation for a full understanding of superconductivity in the AFeSe series of materials.

## Acknowledgments

We thank W. Bao and Z. Y. Lu for helpful discussions. This work was supported by the 973 program under Grant No. 2011CBA00112, by the NSF of China under Grant Nos. 11034012 and 11004243, by the Fundamental Research Funds for Central Universities, and by the Research Funds of Renmin University of China (RUC)(10XNI017, 10XNL016 & 08XNF018). Computational facilities were provided by the HPC Laboratory in the Department of Physics at RUC. The atomic structures and displacement patterns were plotted using the program XCRYSDEN.<sup>29</sup>

- 
- \* Electronic address: qmzhang@ruc.edu.cn
- <sup>1</sup> Y. Kamihara, H. Hiramatsu, M. Hirano, R. Kawamura, H. Yanagi, T. Kamiya, and H. Hosono, *J. Am. Chem. Soc.* **128**, 10012 (2006); X. H. Chen, T. Wu, G. Wu, R. H. Liu, H. Chen, and D. F. Fang, *Nature* **453**, 761 (2008); G. F. Chen, Z. Li, D. Wu, G. Li, W. Z. Hu, J. Dong, P. Zheng, J. L. Luo, and N. L. Wang, *Phys. Rev. Lett.* **100**, 247002 (2008).
  - <sup>2</sup> M. Rotter, M. Tegel, and D. Johrendt, *Phys. Rev. Lett.* **101**, 107007 (2008).
  - <sup>3</sup> X. C. Wang, Q. Q. Liua, Y. X. Lva, W. B. Gao, L. X. Yanga, R. C. Yua, F. Y. Lia, and C. Q. Jin, *Solid State Commun.* **148**, 538 (2008).
  - <sup>4</sup> F.-C. Hsu, J.-Y. Luo, K.-W. Yeh, T.-K. Chen, T.-W. Huang, P. M. Wu, Y.-C. Lee, Y.-L. Huang, Y.-Y. Chu, D.-C. Yan, and M.-K. Wu, *Proc. Natl. Acad. Sci. U.S.A.* **105**, 14262 (2008).
  - <sup>5</sup> X. Y. Zhu, F. Han, G. Mu, P. Cheng, B. Shen, B. Zeng, and H. H. Wen, *Phys. Rev. B* **79**, 220512(R) (2009); G. F. Chen, T. L. Xia, H. X. Yang, J. Q. Li, P. Zheng, J. L. Luo, and N. L. Wang, *Supercond. Sci. Technol.* **22**, 072001 (2009); H. Ogino, Y. Matsumura, Y. Katsura, K. Ushiyama, S. Horii, K. Kishio, and J. Shimoyama, *Supercond. Sci. Technol.* **22**, 075008 (2009).
  - <sup>6</sup> M. K. Wu, F. C. Hsu, K. W. Yeh, T. W. Huang, J. Y. Luo, M. J. Wang, H. H. Chang, T. K. Chen, S. M. Rao, B. H. Mok, C. L. Chen, Y. L. Huang, C. T. Ke, P. M. Wu, A. M. Chang, C. T. Wu, and T. P. Perng, *Physica C* **469**, 340 (2009).
  - <sup>7</sup> S. Margadonna, Y. Takabayashi, Y. Ohishi, Y. Mizuguchi, Y. Takano, T. Kagayama, T. Nakagawa, M. Takata, and K. Prassides, *Phys. Rev. B* **80**, 064506 (2009).
  - <sup>8</sup> J.-G. Guo, S.-F. Jin, G. Wang, S.-C. Wang, K.-X. Zhu, T.-T. Zhou, M. He, and X.-L. Chen, *Phys. Rev. B* **82**, 180520(R) (2010).
  - <sup>9</sup> Z. G. Chen, R. H. Yuan, T. Dong, G. Xu, Y. G. Shi, P. Zheng, J. L. Luo, J. G. Guo, X. L. Chen, and N. L. Wang, unpublished (arXiv:1101.0572); R. H. Yuan, T. Dong, G. F. Chen, J. B. He, D. M. Wang, and N. L. Wang, unpublished (arXiv:1102.1381).
  - <sup>10</sup> W.-Q. Yu, L. Ma, J. B. He, D. M. Wang, T.-L. Xia, and G. F. Chen, arXiv:cond-mat/1101.1017; L. Ma, J. B. He, D. M. Wang, G. F. Chen, W.-Q. Yu, unpublished (arXiv:1101.3687); H. Kotegawa, Y. Hara, H. Nohara, H. Tou, Y. Mizuguchi, H. Takeya, and Y. Takano, unpublished (arXiv:1101.4572); D. A. Torchetti, M. Fu, D. C. Christensen, K. J. Nelson, T. Imai, H. C. Lei, and C. Petrovic, unpublished (arXiv:1101.4967).
  - <sup>11</sup> D. X. Mou, S. Y. Liu, X. W. Jia, J. F. He, Y. Y. Peng, L. Zhao, L. Yu, G. D. Liu, S. L. He, X. L. Dong, J. Zhang, H. D. Wang, C. H. Dong, M. H. Fang, X. Y. Wang, Q. J. Peng, Z. M. Wang, S. J. Zhang, F. Yang, Z. Y. Xu, C. T. Chen, and X. J. Zhou, unpublished (arXiv:1101.4556); X. P. Wang, T. Qian, P. Richard, P. Zhang, J. Dong, H.-D. Wang, C.-H. Dong, M.-H. Fang, and H. Ding, unpublished (arXiv:1101.4923).
  - <sup>12</sup> A. M. Zhang, K. Liu, J. H. Xiao, J. B. He, D. M. Wang, G. F. Chen, B. Normand, and Q. M. Zhang, unpublished (arXiv:1101.2168).
  - <sup>13</sup> Z. Wang, Y. J. Song, H. L. Shi, Z. W. Wang, Z. Chen, H. F. Tian, G. F. Chen, J. G. Guo, H. X. Yang, and J. Q. Li, unpublished (arXiv:1101.2059).
  - <sup>14</sup> W. Bao, Q. Huang, G. F. Chen, M. A. Green, D. M. Wang, J. B. He, X. Q. Wang, and Y. Qiu, unpublished (arXiv:1102.0830); Wei Bao, G. N. Li, Q. Huang, G. F. Chen, J. B. He, M. A. Green, Y. Qiu, D. M. Wang, and J. L. Luo, unpublished (arXiv:1102.3674).
  - <sup>15</sup> R. H. Liu, X. G. Luo, M. Zhang, A. F. Wang, J. J. Ying, X. F. Wang, Y. J. Yan, Z. J. Xiang, P. Cheng, G. J. Ye, Z. Y. Li, and X. H. Chen, unpublished (arXiv:1102.2783).
  - <sup>16</sup> D. H. Ryan, W. N. Rowan-Weetaluktuk, J. M. Cadogan, R. Hu, W. E. Straszheim, S. L. Bud'ko, and P. C. Canfield, unpublished (arXiv:1103.0059); Z.-W. Li, X.-M. Ma, H. Pang, and F.-S. Li, unpublished (arXiv:1103.0098).
  - <sup>17</sup> A. Krzton-Maziopa, Z. Shermadini, E. Pomjakushina, V. Pomjakushin, M. Bendele, A. Amato, R. Khasanov, H. Luetkens, and K. Conder, *J. Phys.: Condens. Matter* **23**, 052203 (2011); Y. Mizuguchi, H. Takeya, Y. Kawasaki, T. Ozaki, S. Tsuda, T. Yamaguchi, and Y. Takano, *Appl. Phys. Lett.* **98**, 042511 (2011); A. F. Wang, J. J. Ying, Y. J. Yan, R. H. Liu, X. G. Luo, Z. Y. Li, X. F. Wang, M. Zhang, G. J. Ye, P. Cheng, Z. J. Xiang, and X. H. Chen, *Phys. Rev. B* **83**, 060512 (2011); M.-H. Fang, H.-D. Wang, C.-H. Dong, Z.-J. Li, C.-M. Feng, J. Chen, and H.-

- Q. Yuan, unpublished (arXiv:1012.5536); J. J. Ying, X. F. Wang, X. G. Luo, A. F. Wang, M. Zhang, Y. J. Yan, Z. J. Xiang, R. H. Liu, P. Cheng, G. J. Ye, and X. H. Chen, unpublished (arXiv:1012.5552); C.-H. Li, B. Shen, F. Han, X.-Y. Zhu, and H.-H. Wen, unpublished (arXiv:1012.5637); H.-D. Wang, C.-H. Dong, Z.-J. Li, S.-S. Zhu, Q.-H. Mao, C.-M. Feng, H.-Q. Yuan, and M.-H. Fang, *Europhys. Lett.* **93**, 47004 (2011).
- <sup>18</sup> Z.-A. Ren, G.-C. Che, X.-L. Dong, J. Yang, W. Lu, W. Yi, X.-L. Shen, Z.-C. Li, L.-L. Sun, F. Zhou, and Z.-X. Zhao, *Europhys. Lett.* **83**, 17002 (2008); C. Wang, L.-J. Li, S. Chi, Z.-W. Zhu, Z. Ren, Y.-K. Li, Y.-T. Wang, X. Lin, Y.-K. Luo, S. Jiang, X.-F. Xu, G.-H. Cao, and Z.-A. Xu, *Europhys. Lett.* **83**, 67006 (2008).
- <sup>19</sup> D. M. Wang, J. B. He, T.-L. Xia, and G. F. Chen, unpublished (arXiv:1101.0789).
- <sup>20</sup> W. Bao, G. N. Li, Q. Huang, G. F. Chen, J. B. He, M. A. Green, Y. Qiu, D. M. Wang, and J. L. Luo, unpublished (arXiv:1102.3674).
- <sup>21</sup> G. Kresse and J. Hafner, *Phys. Rev. B* **47**, 558 (1993); G. Kresse and J. Furthmüller, *Phys. Rev. B* **54**, 11169 (1996).
- <sup>22</sup> P. E. Blöchl, *Phys. Rev. B* **50**, 17953 (1994); G. Kresse and D. Joubert, *Phys. Rev. B* **59**, 1758 (1999).
- <sup>23</sup> J. P. Perdew, K. Burke, and M. Ernzerhof, *Phys. Rev. Lett.* **77** 3865 (1996).
- <sup>24</sup> K. Liu and S. Gao, *Phys. Rev. Lett.* **95**, 226102 (2005).
- <sup>25</sup> A. P. Litvinchuk, V. G. Hadjiev, M. N. Iliev, Bing Lv, A. M. Guloy, and C. W. Chu, *Phys. Rev. B* **78**, 060503 (2008).
- <sup>26</sup> P. E. Sulewski, P. A. Fleury, K. B. Lyons, and S.-W. Cheong, *Phys. Rev. Lett.* **67**, 3864 (1991).
- <sup>27</sup> S. Chakravarty, R. B. Laughlin, D. K. Morr, and C. Nayak, *Phys. Rev. B* **63**, 094503 (2001).
- <sup>28</sup> P. Zavalij, W. Bao, X. F. Wang, J. J. Ying, X. H. Chen, D. M. Wang, J. B. He, X. Q. Wang, G. F. Chen, P.-Y. Hsieh, Q. Huang, and M. A. Green, unpublished (arXiv:1101.4882).
- <sup>29</sup> A. Kokalj, *Comp. Mater. Sci.* **28**, 155 (2003). Code available from <http://www.xcrysden.org/>.